Coherent control of cross-peaks in chirality-induced two-dimensional optical signals of excitons

Dmitri V. Voronine, Darius Abramavicius, and Shaul Mukamel
Department of Chemistry, University of California, Irvine, California 92697-2025

(Received 15 August 2006; accepted 23 October 2006; published online 14 December 2006)

Polarization tuning of the interference of chirality-induced tensor components is used to simulate the suppression of diagonal peaks and amplification of cross peaks in femtosecond two-dimensional photon echo signals of excitons in a chiral porphyrin dimer. Superpositions of various tensor components which generate the optimized signals are constructed using a genetic learning algorithm. Exciton couplings and bath correlations may be extracted from these highly resolved signals. © *2006 American Institute of Physics*. [DOI: 10.1063/1.2397686]

Two-dimensional coherent photon echoes (2D PE) in the visible offer new possibilities for the study of excitons.[1,2] Inhomogeneous and homogeneous fluctuations, exciton relaxation pathways, and energy correlation functions can be directly probed. These effects were demonstrated in recent experiments on photosynthetic complexes.[3–6] The corresponding infrared techniques have been applied to study protein folding.[7–9]

Controlling the polarizations of incoming laser pulses may be utilized to fine-tune 2D PE signals. Selection rules for the various polarization tensors have been established long ago[10] but were only recently investigated within the dipole approximation in 2D PE experiments.[11,12] It was demonstrated that specific configurations of pulse polarizations could eliminate diagonal peaks in 2D PE, thereby amplifying the desired cross peaks[13] and discriminating between polypeptide secondary structures.[14]

We have recently predicted a new family of chirality-induced (CI) 2D PE signals based on polarization configurations calculated to first order in the optical wave vectors.[15] The third-order CI signals constitute a nonlinear extension of the most common linear chirality-sensitive spectroscopic tool, circular dichroism (CD),[16] which is extensively used, for instance, in protein structure determination[17] and in the characterization of light harvesting systems.[18] Like CD, the nonlinear optical CI signals vanish in nonchiral systems and in racemic mixtures.

Polarization control affects the constructive/destructive interference of various tensor components of response functions. Recent progress in pulse shaping technology allows the design of laser pulses for specific targets[19] and the active control of quantum-mechanical systems.[20] Phase, amplitude, and polarization-shaped pulses can manipulate the polarization-sensitive density matrix Liouville space pathways of the quantum evolution.[21,22] Applying polarization shaping to CI third-order signals opens up new opportunities for the control of multidimensional signals of excitons by controlling 2D peak amplitudes and amplifying desired features.[23] These tensor components can be directly observed by heterodyne detection.[24]

In this paper we demonstrate the power of these techniques by using a simplified algorithm where superpositions of the various tensor components are optimized. We employ a genetic algorithm to amplify selected peaks in optical CI signals from a chiral porphyrin dimer, whose CD spectra have been used as sensors of chiral systems.[32]

The Frenkel exciton Hamiltonian and the crystal structure parameters (interchromophore distance and the coordinates of the electric transition dipoles) of the "complex 5" dimer of Zn porphyrin were taken from Won *et al.*[25] Matrix elements of the one-exciton Hamiltonian are given in Table I A. The transition electric dipoles of the monomers which pass through the nitrogens [Fig. 1(a)] are given in Table I B, while the transition dipole positions are given in Table I C.

The relevant eigenstates form three manifolds [Fig. 1(b)]: the ground state (g), four single-exciton states (e,e'), and six two-exciton states (f). Only the g to e and the e to f transitions are allowed. The one- and the two-exciton eigenstates with frequencies Ω_i and Ω_i', respectively, were obtained by diagonalizing the corresponding blocks of the

TABLE I. (A) One-exciton Hamiltonian matrix elements (in cm^{-1}) for a chiral porphyrin dimer. (B) Electric transition dipole vectors (Debye). (C) Coordinates of the electric transition dipoles (Å).

		B_{1x}	B_{2x}	B_{1y}	B_{2y}
A	B_{1x}	24 631	495	0	490
	B_{2x}	495	24 631	306	0
	B_{1y}	0	306	24 631	487
	B_{2y}	490	0	487	24 631
B		μ_x	μ_y	μ_z	
	B_{1x}	7.57	4.34	−6.2	
	B_{2x}	−8.26	2.82	−6.2	
	B_{1y}	7.57	−4.34	6.2	
	B_{2y}	−1.73	8.55	6.2	
C		$\mathbf{r}_x$	$\mathbf{r}_y$	$\mathbf{r}_z$	
	B_{1x}	0	0	0	
	B_{2x}	0	0	10.5	
	B_{1y}	0	0	0	
	B_{2y}	0	0	10.5	

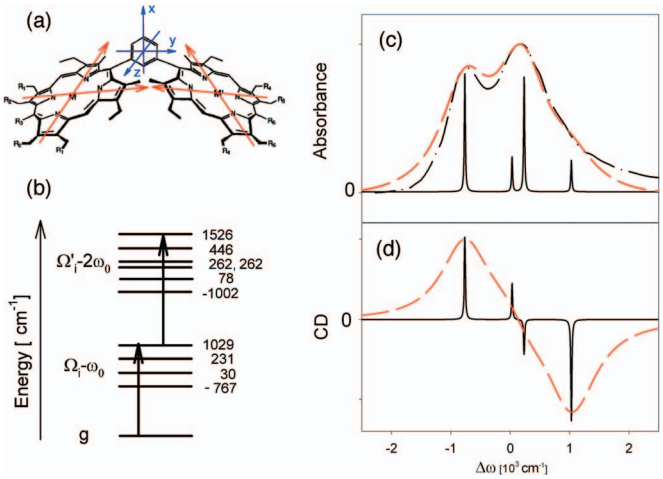

FIG. 1. (Color) (a) Structure of a chiral porphyrin dimer. $M=M'=$Zn. [Adapted from Won *et al.* (Ref. 25).] The interchromophore distance is 10.5 Å, the dihedral angle is 132°. (b) The exciton level scheme: the ground state, four single-exciton states at $\Delta\Omega_1=-767$ cm^{-1}, $\Delta\Omega_2=30$ cm^{-1}, $\Delta\Omega_3=231$ cm^{-1}, and $\Delta\Omega_4=1029$ cm^{-1} (where $\Delta\Omega_i=\Omega_i-\omega_0$), and six two-exciton states at $\Delta\Omega'_1=-1002$ cm^{-1}, $\Delta\Omega'_2=78$ cm^{-1}, $\Delta\Omega'_3=262$ cm^{-1}, $\Delta\Omega'_4=262$ cm^{-1}, $\Delta\Omega'_5=446$ cm^{-1}, $\Delta\Omega'_6=1526$ cm^{-1} (where $\Delta\Omega'_i=\Omega'_i-2\omega_0$) with $\omega_0=24500$ cm^{-1}. (c) Linear absorption of the porphyrin dimer: experimental (dash-dotted black) (Ref. 25), simulated with $\Gamma=500$ cm^{-1} (dashed red), and $\Gamma=10$ cm^{-1} (solid black). (d) Simulated circular dichroism with $\Gamma=500$ cm^{-1} (dashed red) and $\Gamma=10$ cm^{-1} (solid black).

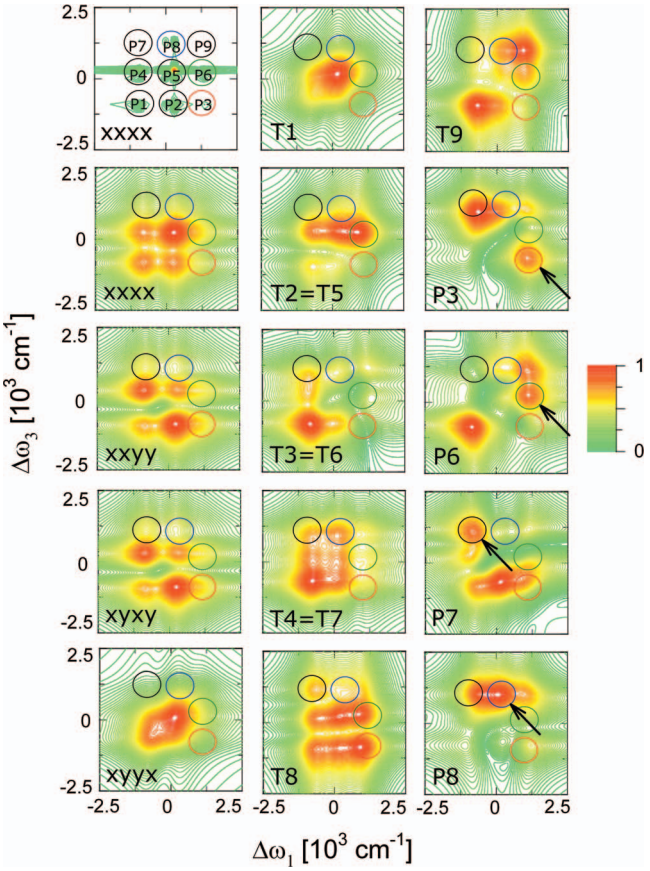

FIG. 2. (Color) Absolute magnitude of 2D signals of the porphyrin dimer: four nonchiral tensor components *xxxx*, *xxyy*=*xyxy*, *xyyx*, nine chiral components T_1-T_9, and optimized linear combinations P_3, P_6, P_7, and P_8, highlighted with red, green, black, and blue circles, respectively. Optimized peaks are marked by arrows. The top left panel shows the *xxxx* signal calculated with $\Gamma=10$ cm^{-1} where all peaks are resolved.

Hamiltonian. The absorption, CD, and third-order signals are calculated using the method described in Ref. 23.

The Soret band of the dimer consists of two pairs of degenerate perpendicular transition dipoles: B_{1x}, B_{1y} and B_{2x}, B_{2y}, where the indices 1 and 2 label the monomers and x and y are the polarization directions. The linear absorption [Fig. 1(c)] simulated with a homogeneous dephasing rate $\Gamma=500$ cm^{-1} (dashed red) provides a good fit to experiment (dash-dotted black). For peak assignments we further show a stick ($\Gamma=10$ cm^{-1}) spectrum (solid black). The corresponding simulated circular dichroism spectra are shown in Fig. 1(d). The four single-exciton transitions, are not resolved in these spectra due to the large broadening.

The third-order 2D PE signal of the Soret band generated at $\mathbf{k}_s=-\mathbf{k}_1+\mathbf{k}_2+\mathbf{k}_3$, where $\mathbf{k}_1$, $\mathbf{k}_2$, $\mathbf{k}_3$, and $\mathbf{k}_S$ are the wave vectors of the first, second, third, and the signal pulses, respectively, is a linear superposition of various tensor components of the response function $\mathbb{R}^{\mathbf{k}_I=-\mathbf{k}_1+\mathbf{k}_2+\mathbf{k}_3}_{\nu_4\nu_3\nu_2\nu_1}(\omega_3,t_2=+0,\omega_1)$.[23] Here $\boldsymbol{\nu}_j$ are the pulse polarizations. For simplicity we set the waiting time $t_2=0$ in the present calculations. Exciton population transport which takes place during t_2 will be an interesting subject of a future study. The response functions were simulated using the nonlinear exciton equation approach.[26] The nonchiral (NC) tensor components (dipole approximation) are displayed in the first column in Fig. 2. These include $\nu_4\nu_3\nu_2\nu_1\equiv xxyy$, *xyxy*, and *xyyx* (Ref. 27) (*xxxx* is given by the sum of the three: *xxxx*=*xxyy*+*xyxy*+*xyyx*). To identify the possible resonances, *xxxx* in the top left panel was calculated with $\Gamma=10$ cm^{-1}. These resonances assigned in Table II represent one-exciton transitions $(-\Omega_a,\Omega_a)$ (diagonal peaks), correlations between states $(-\Omega_a,\Omega_b)$ with $a\neq b$, and transitions between one- and two-exciton states $(-\Omega_a,\Omega'_b-\Omega_a)$ (cross peaks). The spectra show three diagonal and six off-diagonal peaks labeled P_1-P_9.

The diagonal peaks P_1 and P_5 and the cross peaks P_2 and P_4 are the most prominent features, in these NC components. The nine linearly independent CI tensor components calculated to first order in the wave vector[27] are shown in Fig. 2 (second and third columns). These are labeled $T_1=\mathbb{R}_{xyzx}(z,x,\bar{x},\bar{z})$, $T_2=\mathbb{R}_{xyxz}(z,x,z,x)$, $T_3=\mathbb{R}_{xyxx}(z,z,z,z)$, $T_4=\mathbb{R}_{xyxx}(z,z,y,y)$, $T_5=\mathbb{R}_{xxyz}(z,z,x,x)$, $T_6=\mathbb{R}_{xxyx}(z,z,z,z)$, $T_7=\mathbb{R}_{xxyx}(z,y,z,y)$, $T_8=\mathbb{R}_{xxxy}(z,z,z,z)$, and $T_9=\mathbb{R}_{xxxy}(z,y,\bar{y},\bar{z})$. Here $\mathbb{R}_{\nu_4\nu_3\nu_2\nu_1}(\kappa_4,\kappa_3,\kappa_2,\kappa_1)\equiv\mathbb{R}^{\mathbf{k}_I=-\mathbf{k}_1+\mathbf{k}_2+\mathbf{k}_3}_{\nu_4\nu_3\nu_2\nu_1}(\omega_3,t_2=+0,\omega_1)$ denotes the CI tensor component with polarization directions $\boldsymbol{\nu}_j$ and wave vector directions $\boldsymbol{\kappa}_j$, $j=1,2,3,s$. For the present calculations $T_2=T_5$, $T_3=T_6$, and $T_4=T_7$ since the second delay period $t_2=0$. The CI components reveal new peak patterns not observed in the NC tensor components. Some CI components amplify weak peaks in the NC spectra: P_6 in T_2, T_5, and T_8, P_3 in T_8, and P_9 in T_9. The excitonic quadrupoles make a very small contribution to the NC components but are the leading terms for the CI components. Magnetic contributions were neglected. Measuring all tensor components should allow, therefore, to distinguish between these various interactions.

The control targets considered below are aimed at manipulating these peaks. To that end we have constructed the

TABLE II. 2D photon echo resonances for the porphyrin dimer identified for *xxxx* ($\Gamma=10$ cm^{-1}) in Fig. 2.

ω_3 resonances	$\omega_1=-\Omega_1$	$\omega_1=-\Omega_2$	$\omega_1=-\Omega_3$	$\omega_1=-\Omega_4$
1	$(-\Omega_1,\Omega_1)$	$(-\Omega_2,\Omega_1)$	$(-\Omega_3,\Omega_1)$	$(-\Omega_4,\Omega_1)$
	$(-\Omega_1,\Omega_3'-\Omega_4)$	$(-\Omega_2,\Omega_3'-\Omega_4)$	$(-\Omega_3,\Omega_3'-\Omega_4)$	$(-\Omega_4,\Omega_3'-\Omega_4)$
	$(-\Omega_1,\Omega_4'-\Omega_4)$	$(-\Omega_2,\Omega_4'-\Omega_4)$	$(-\Omega_3,\Omega_4'-\Omega_4)$	$(-\Omega_4,\Omega_4'-\Omega_4)$
2	$(-\Omega_1,\Omega_1'-\Omega_1)$	$(-\Omega_2,\Omega_1'-\Omega_1)$	$(-\Omega_3,\Omega_1'-\Omega_1)$	$(-\Omega_4,\Omega_1'-\Omega_1)$
3	$(-\Omega_1,\Omega_2'-\Omega_3)$	$(-\Omega_2,\Omega_2'-\Omega_3)$	$(-\Omega_3,\Omega_2'-\Omega_3)$	$(-\Omega_4,\Omega_2'-\Omega_3)$
4	$(-\Omega_1,\Omega_3'-\Omega_3)$	$(-\Omega_2,\Omega_3'-\Omega_3)$	$(-\Omega_3,\Omega_3'-\Omega_3)$	$(-\Omega_4,\Omega_3'-\Omega_3)$
	$(-\Omega_1,\Omega_4'-\Omega_3)$	$(-\Omega_2,\Omega_4'-\Omega_3)$	$(-\Omega_3,\Omega_4'-\Omega_3)$	$(-\Omega_4,\Omega_4'-\Omega_3)$
	$(-\Omega_1,\Omega_2)$	$(-\Omega_2,\Omega_2)$	$(-\Omega_3,\Omega_2)$	$(-\Omega_4,\Omega_2)$
5	$(-\Omega_1,\Omega_5'-\Omega_2)$	$(-\Omega_2,\Omega_5'-\Omega_2)$	$(-\Omega_3,\Omega_5'-\Omega_2)$	$(-\Omega_4,\Omega_5'-\Omega_2)$
6	$(-\Omega_1,\Omega_2'-\Omega_1)$	$(-\Omega_2,\Omega_2'-\Omega_1)$	$(-\Omega_3,\Omega_2'-\Omega_1)$	$(-\Omega_4,\Omega_2'-\Omega_1)$
7	$(-\Omega_1,\Omega_5'-\Omega_1)$	$(-\Omega_2,\Omega_5'-\Omega_1)$	$(-\Omega_3,\Omega_5'-\Omega_1)$	$(-\Omega_4,\Omega_5'-\Omega_1)$
	$(-\Omega_1,\Omega_6'-\Omega_4)$	$(-\Omega_2,\Omega_6'-\Omega_4)$	$(-\Omega_3,\Omega_6'-\Omega_4)$	$(-\Omega_4,\Omega_6'-\Omega_4)$

following superposition of linearly independent response function tensor components:

$$\mathcal{W}(\omega_1,\omega_3)=\sum_{j=1}^{9} c_j T_j, \tag{1}$$

where c_j are complex coefficients. To define the optimization targets we first introduce the integrated intensity of the jth peak,

$$I_j \equiv \int_{-\delta}^{\delta} d\omega_1 \int_{-\delta}^{\delta} d\omega_3 |\mathcal{W}(\omega_1+\omega_1^j,\omega_3+\omega_3^j)|, \tag{2}$$

where $\delta=212.5$ cm^{-1}. We have varied $c_i=c_i'+ic_i''$ in order to optimize the ratios of the amplitudes of selected peaks. The weakest peaks in the *xxxx* spectrum, P_3, P_6, P_7, and P_8, were targeted for amplification by maximizing the following ratios of intensities—P_3: $I_3/(I_2+I_5+I_6)$, P_6: $I_6/(I_3+I_5+I_9)$, P_7: $I_7/(I_4+I_5+I_8)$, and P_8: $I_8/(I_5+I_7+I_9)$. In each target we divide the integrated intensity of the desired target peak by the sum of overlapping neighboring peaks.

The full optimization results obtained by using the nine CI tensor components in Eq. (1) are shown in Fig. 2 (third column, panels P_3, P_6, P_7, and P_8). The corresponding real and imaginary parts of the 2D signals are shown in supporting Figs. S1, A, and B, respectively.[28] As an initial guess we used $c_{i0}'=c_{i0}''=1/\sqrt{18}$. The optimization was carried out using a genetic algorithm (GA) as described in Refs. 29–31. We varied $c_i' \in [-c_{i0}', c_{i0}']$ and $c_i'' \in [-c_{i0}'', c_{i0}'']$ with the normalization $\Sigma_{i=1}^{9}|c_i|^2=1$ until convergence, when the change of the average cost of the population of GA was less than 0.1%. Convergence was achieved within 1000–2000 generations. The optimization targets for P_3, P_6, P_7, and P_8 were amplified by a factor of 8.0, 6.3, 4.4, and 2.0, respectively, compared to the *xxxx* spectrum. The optimal coefficients c_i are given in Table III.

The optimization of CI tensor components provides a significant improvement in the resolution of congested spectra by the amplification of weak peaks. (P_3) shows the amplification and resolution of the cross peak P_3 due to elimination of the P_2 and P_6 cross peaks and the diagonal peak

TABLE III. Optimized coefficients $c_i=c_i'+ic_i''$ which enhance the peaks P_3, P_6, P_7, and P_8.

P_3	1	2	3	4	5	6	7	8	9
C_i'	0.1112	−0.0501	−0.435	0.1453	−0.1437	−0.3913	0.3895	0.0401	0.1507
C_i''	0.3976	−0.0783	0.1165	−0.2507	−0.3446	−0.2216	0.3533	0.1361	−0.2459
P_6	1	2	3	4	5	6	7	8	9
C_i'	0.1661	0.1028	−0.2126	0.0765	−0.2906	0.0740	0.1936	0.0583	0.1821
C_i''	−0.0625	0.0701	−0.3690	−0.1088	−0.1622	0.4764	−0.1856	−0.4788	0.2702
P_7	1	2	3	4	5	6	7	8	9
C_i'	0.2497	0.0673	−0.1696	0.3185	0.2154	−0.0404	−0.1638	0.1134	0.3676
C_i''	0.3854	0.3179	−0.1955	−0.3611	−0.0660	0.3349	−0.0423	−0.0112	0.2083
P_8	1	2	3	4	5	6	7	8	9
C_i'	0.3188	0.0657	0.1038	0.1082	0.0643	0.0004	0.3095	−0.1645	−0.1946
C_i''	−0.0237	0.3958	−0.3885	0.1839	−0.2360	0.3938	−0.3710	−0.0090	0.1276

P_5. P_6 was enhanced by eliminating the diagonal peak P_5 and the cross peak P_3 and by suppressing the diagonal peak P_9. Similarly, the cross peaks P_7 and P_8 were amplified. The cross peak P_8 and the diagonal peak P_5 were eliminated, and the cross peak P_4 was suppressed. The cross peak P_7 and the diagonal peak P_9 were suppressed, and the diagonal peak P_5 was eliminated (P_8).

We have also optimized the superposition of the three nonchiral tensor components: *xxyy*, *xyyx*, and *xyxy*, and found that they cannot resolve these peaks. Optimization (not shown) results in a small amplification of P_3, P_6, P_7, and P_8 by a factor of 1.3, 2.1, 1.3, and 1.8, respectively. P_6 is amplified as a result of the partial suppression of the diagonal peaks P_5 and P_9.

In summary, we have simulated the CI photon echo signals ($\mathbf{k}_I=-\mathbf{k}_1+\mathbf{k}_2+\mathbf{k}_3$) for a porphyrin dimer calculated to first order in $\mathbf{k}$. By taking a linear superposition of CI tensor components we amplified these cross peaks and eliminated the diagonal peaks P_1, P_5, and P_9. Linear combinations of CI tensor components are required for the elimination/amplification of various peaks. Polarization-controlled experiments[19,20] may be designed to directly search for and measure the optimized linear combinations rather than measuring each component separately followed by data processing, as done here. The nonchiral tensor components of the response function do not achieve a similar degree of control.

This research was supported by the National Science Foundation Grant No. CHE-0446555 and the National Institutes of Health 2RO1-GM59230-05. The authors wish to thank T. Brixner for valuable discussions.

[1] T. Meier, V. Chernyak, and S. Mukamel, J. Chem. Phys. **107**, 8759 (1997).
[2] S. Mukamel, Annu. Rev. Phys. Chem. **51**, 691 (2000).
[3] T. Brixner, I. V. Stiopkin, and G. R. Fleming, Opt. Lett. **29**, 884 (2004).
[4] B. S. Prall, D. Y. Parkinson, and G. R. Fleming, J. Chem. Phys. **123**, 054515 (2005).
[5] T. Brixner, J. Stenger, H. Vaswani, M. Cho, R. Blankenship, and G. Fleming, Nature (London) **434**, 625 (2004).
[6] M. Cho, H. M. Vaswani, T. Brixner, J. Stenger, and G. R. Fleming, J. Phys. Chem. B **109**, 10542 (2005).
[7] I. V. Rubstov, J. Wang, and R. M. Hochstrasser, Proc. Natl. Acad. Sci. U.S.A. **100**, 5601 (2003).
[8] C. Fang, J. Wang, Y. S. Kim, A. K. Charnley, W. Barber-Armstrong, A. B. Smith III, S. M. Decatur, and R. M. Hochstrasser, J. Phys. Chem. B **108**, 10415 (2004).
[9] H. Chung, M. Khalil, A. W. Smith, Z. Ganim, and A. Tokmakoff, Proc. Natl. Acad. Sci. U.S.A. **102**, 612 (2005).
[10] D. L. Andrews and T. Thirunamachandran, J. Chem. Phys. **67**, 5026 (1977).
[11] R. M. Hochstrasser, Chem. Phys. **266**, 273 (2001).
[12] O. Golonzka and A. Tokmakoff, J. Chem. Phys. **115**, 297 (2001).
[13] M. T. Zanni, N.-H. Ge, Y. S. Kim, and R. M. Hochstrasser, Proc. Natl. Acad. Sci. U.S.A. **98**, 11265 (2001).
[14] H. Maekawa, C. Toniolo, A. Moretto, Q. B. Broxterman, and N.-H. Ge, J. Phys. Chem. B **110**, 5834 (2006).
[15] D. Abramavicius and S. Mukamel, J. Chem. Phys. **122**, 1 (2005).
[16] *Circular Dichroism. Principles and Applications*, 2nd ed., edited by N. Berova, K. Nakanishi, and R. W. Woody (Wiley, New York, 2000).
[17] R. Woody and N. Sreerama, J. Chem. Phys. **111**, 2844 (1999).
[18] S. Georgakopoulou, R. Frese, E. Johnson, C. Koolhaas, R. Cogdell, R. van Grondelle, and G. van der Zwan, Biophys. J. **82**, 2184 (2002).
[19] T. Brixner, N. H. Damrauer, G. Krampert, P. Niklaus, and G. Gerber, J. Opt. Soc. Am. B **20**, 878 (2003).
[20] T. Brixner, N. H. Damrauer, G. Krampert, P. Niklaus, and G. Gerber, J. Mod. Opt. **50**, 539 (2003).
[21] T. Brixner, G. Krampert, T. Pfeifer, R. Selle, G. Gerber, M. Wollenhaupt, O. Graefe, C. Horn, D. Liese, and T. Baumert, Phys. Rev. Lett. **92**, 208301 (2004).
[22] G. Vogt, G. Krampert, P. Niklaus, P. Nuernberger, and G. Gerber, Phys. Rev. Lett. **94**, 068305 (2005).
[23] D. Abramavicius and S. Mukamel, J. Chem. Phys. **124**, 034113 (2006).
[24] S. Mukamel, *Principles of Nonlinear Optical Spectroscopy* (Oxford University Press, New York, 1995).
[25] Y. Won, R. Friesner, M. Johnson, and J. Sessler, Photosynth. Res. **22**, 201 (1989).
[26] V. Chernyak, W. M. Zhang, and S. Mukamel, J. Chem. Phys. **109**, 9587 (1998).
[27] D. Abramavicius, W. Zhuang, and S. Mukamel, J. Phys. B **39**, 5051 (2006)..
[28] See EPAPS Document No. E-JCPSA6-125-504646 for Figs. S1 A, B. Figure S1 shows the real (A) and imaginary (B) parts of the 2D signals of the porphyrin dimer: 4 nonchiral tensor components *xxxx*, *xxyy*=*xyxy*, *xyyx*; 9 chiral components T1-T9; optimized linear combinations P3, P6, P7, and P8. This document can be reached via a direct link in the online article's HTML reference section or via the EPAPS homepage (http://www.aip.org/pubservs/epaps.html).
[29] D. Zeidler, S. Frey, K.-L. Kompa, and M. Motzkus, Phys. Rev. A **64**, 023420 (2001).
[30] D. Abramavicius and S. Mukamel, J. Chem. Phys. **120**, 8373 (2004).
[31] D. Voronine, D. Abramavicius, and S. Mukamel, J. Chem. Phys. **124**, 034104 (2006).
[32] J.-C. Marchon and R. Ramasseul, Porphyrin Handbook **11**, 75 (2003).